JOURNAL OF GEOPHYSICAL RESEARCH, VOL. 113, A02210, doi:10.1029/2007JA012736, 2008

Pickup oxygen ion velocity space and spatial distribution around Mars

Xiaohua Fang,[1,2] Michael W. Liemohn,[1] Andrew F. Nagy,[1] Yingjuan Ma,[1,3] Darren L. De Zeeuw,[1] Janet U. Kozyra,[1] and Thomas H. Zurbuchen[1]

Received 17 August 2007; revised 30 October 2007; accepted 19 November 2007; published 22 February 2008.

[1] We report a newly created highly parallelized global test particle model for resolving the pickup oxygen ion distribution around Mars. The background magnetic and convection electric fields are calculated using a three-dimensional multispecies magnetohydrodynamic model, which includes the effect of the Martian crustal magnetic field. In addition to photo-ionization, charge exchange collisions and solar wind electron impact ionization are included for the pickup ion generation. The most novel feature of our model is that more than one billion test particles are launched in the simulation domain in total. This corresponds to a profound enhancement by at least 3 orders of magnitude in the total number, compared to all existing test particle models. This substantial improvement enables an unprecedented examination of the pickup ion flux distribution in velocity space, which is not achievable in previous simulation studies due to the insufficient statistics arising from the limited number of test particles. Using the velocity space distribution of pickup O^+ ions as a tool, the Mars-solar wind interaction can be investigated in a unique way. It is shown that the velocity space distribution is highly non-Maxwellian, exhibiting non-gyrotropic and non-symmetric distributions, including many beam-like features. In the tail region, pickup ions have a prominent outflowing component in the whole energy range. The energy examination of particles traveling across the tail region shows that the acceleration highly depends on the source region where the particles originate. The strong convection electric field in the magnetosheath region is favorable to the pickup ion acceleration.

Citation: Fang, X., M. W. Liemohn, A. F. Nagy, Y. Ma, D. L. De Zeeuw, J. U. Kozyra, and T. H. Zurbuchen (2008), Pickup oxygen ion velocity space and spatial distribution around Mars, *J. Geophys. Res.*, *113*, A02210, doi:10.1029/2007JA012736.

1. Introduction

[2] Without the shielding of a strong intrinsic magnetic field, the Martian atmosphere directly interacts with the impacting solar wind plasma. This proximity, and in fact overlap, between the solar wind and the planetary neutral environment create a scenario where particles can be stripped away from the Martian atmosphere and lost to deep space. Martian ion pickup and consequent mass loading of the solar wind have been the subject of great interest in scientific research, because they represent the complex interaction between the unmagnetized planet and the solar wind.

[3] There are three ways ions of planetary origin can be generated. The neutral atmospheric constituents can be ionized by solar radiation. The charge exchange collisions with ions as well as the impact ionization by solar wind electrons are another two mechanisms responsible for the generation of planetary ions. Once atmospheric atoms and molecules become ionized, the newly created ions are picked up by the interplanetary magnetic field (IMF) and the convection electric field. As a consequence of the momentum transfer by electromagnetic fields from the solar wind to the pickup ions, mass loading effectively slows down the solar wind around Mars.

[4] The current global models of the Mars-solar wind interaction have been recently reviewed by *Nagy et al.* [2004]. One approach to describe the physical processes controlling the interaction of the solar wind plasma with the Martian atmosphere and ionosphere is to use the magneto-hydrodynamic (MHD) equations. The plasma flow is either regarded as a single fluid with multiple species [*Liu et al.*, 1999; *Ma et al.*, 2002, 2004], or as a multifluid (solar wind proton and heavy planetary ion) system [*Sauer et al.*, 1990; *Sauer and Dubinin*, 2000; *Harnett and Winglee*, 2006]. The MHD models have been successful, in general, to reproduce many observed features, such as the locations of the bow shock (BS) and the ionopause, for example. However, ion motion in the Martian environment distinctly differs from that in the Earth case. That is, due to the lack of a strong

[1]Space Physics Research Laboratory, University of Michigan, Ann Arbor, Michigan, USA.
[2]Now at Laboratory for Atmospheric and Space Physics, University of Colorado, Boulder, Colorado, USA.
[3]Now at Institute of Geophysics and Planetary Physics, University of California, Los Angeles, Los Angeles, California, USA.

0148-0227/08/2007JA012736$09.00

intrinsic magnetic field, the gyroradius of a pickup ion can be very large, which is comparable to or even larger than the planetary scale. The fluid approximation in the MHD models therefore cannot resolve the kinetic effects of ion dynamics. For example, the asymmetric planetary ion distribution is not reproduced in the MHD models.

[5] On the other hand, the Mars-solar wind interaction has also been modeled using a semi-kinetic (hybrid) approach. In hybrid particle simulations, ions are considered as individual particles and electrons are treated as a massless, charge-neutralizing fluid [*Brecht et al.*, 1993; *Brecht*, 1997; *Kallio and Janhunen*, 2002; *Modolo et al.*, 2005]. The hybrid approach is often considered particularly suitable for global modeling of the interaction of the solar wind with Mars. However, in practice, limitations in computational speed and computer memory in hybrid simulations necessitate a number of simplifications and assumptions. The number of ions per cell is low (usually no more than tens of particles), making it very difficult to accurately achieve statistical behaviors and perform detailed chemistry calculations.

[6] As an attractive alternative, test particle simulations are widely used to investigate the pickup ion distribution around Mars. The particle transport is modeled within the magnetic field and convection electric field that are obtained either by a gas dynamic magnetosheath model [*Luhmann and Schwingenschuh*, 1990], a combined model of a gas dynamic magnetosheath and a comet-like magnetotail [*Luhmann*, 1990; *Lichtenegger et al.*, 1995; *Lichtenegger and Dubinin*, 1998], an empirical model based on the Phobos 2 spacecraft measurements [*Kallio and Koskinen*, 1999], or an MHD model [*Cravens et al.*, 2002]. The test particle simulations succeeded in resolving the asymmetric spatial pickup ion distribution by taking into account the finite gyroradius effects of the ions while reducing statistical noise at the same time by using a large number of test particles.

[7] The aforementioned test particle models are appropriate for describing the spatial distribution of pickup ions around Mars. However, due to the limitation of computational resources available at that time, the number of test particles launched in the simulations were not enough to accurately resolve the full velocity space distribution at any given spatial points. By full velocity space distribution, we mean the pickup ion distribution versus particle energy and velocity direction. For example, in the studies of *Kallio and Koskinen* [1999] and *Cravens et al.* [2002], 5000 and 10^6 test particles in total were released respectively. As can be seen later in this paper, we compare the velocity space distribution results using a variety of test particle numbers, showing that 10^6 particles still provide insufficient resolution to assess the pickup ion flux in full velocity space. Note that *Cravens et al.* [2002] did determine the ion flux versus energy distribution (albeit not full velocity space distribution) at several locations around Mars and their paper made specific and quantitative comparisons with measured ion fluxes by the Phobos 2 spacecraft. The focus of the *Cravens et al.* [2002] paper was on the higher energy ions picked up upstream of the bow shock.

[8] Another limitation of previous test particle models is that the Martian crustal magnetic field [*Acuña et al.*, 1998] was not incorporated into the calculation of the background electromagnetic fields. It has been known that the Martian magnetic anomaly pattern is important for the ionospheric density distribution, the bow shock standoff location, and escaping particle fluxes [*Ma et al.*, 2004; *Ma and Nagy*, 2007]. It is thus expected that the crustal magnetic field will also manifest itself in the pickup ion distribution around Mars. At low altitudes, the localized remanent magnetic field controls particle motion by shielding some regions and focusing the energy input into other regions. However, these effects are not yet investigated in previous studies.

[9] In this paper, we report a newly created highly parallelized test particle model to accurately resolve the Martian pickup oxygen ion distribution in velocity space. One of the novel features of this model is that more than 10^9 test particles are launched in total. This total number is a factor of at least 10^3 to 10^5 more than that in the previous studies, indicating a dramatic improvement in the resolution. As will be illustrated later, the velocity space information can provide a unique and useful way to understand the Mars-solar wind interaction. Moreover, we include photo-ionization, charge exchange collisions with ions, and the solar wind electron impact ionization to produce pickup oxygen ion sources. In addition, a sophisticated three-dimensional (3-D) MHD model (with the crustal magnetic field considered) [*Ma et al.*, 2004] is employed to supply the Martian electromagnetic environment, in which the motion of an individual test particle is traced.

[10] An overview of this paper follows. In section 2, a model description is provided, including a brief introduction to the MHD model of *Ma et al.* [2004] and a detailed information on the test particle model set up. In section 3, the pickup O^+ flux distribution results are presented along the tail. As an example, the trajectory plots of low and high energy ions passing through a spatial location far down the tail are provided for understanding the resolved velocity space distribution. In section 4, the usage of this flux analysis as a tool to probe the Mars-solar wind interaction is discussed by considering the change of the flux distribution. An example is presented by artificially intensifying the Martian electromagnetic fields. Finally, the paper's findings are summarized in section 5.

2. Model Description

2.1. The Mars MHD Model

[11] Our new test particle model employs the global magnetic and electric field calculations of the Mars MHD code of *Ma et al.* [2004]. It is a 3-D, non-ideal, multispecies, single-fluid MHD model, solving for the bulk plasma parameters everywhere in the vicinity of Mars. As the detailed description has been reported by *Ma et al.* [2004], this paper only provides a summary of the main features.

[12] The *Ma et al.* [2004] model solves the conservative form of the MHD equations using four continuity equations (with separate solutions for the mass densities of H^+, O^+, O_2^+, and CO_2^+) and single momentum and energy equations (that is, single plasma velocities and temperatures in the fluid). The magnetic field transport is calculated self-consistently with the plasma solution. The ion chemistry used is reasonably complete for an accurate representation of the source and sink terms for each ion species, as outlined

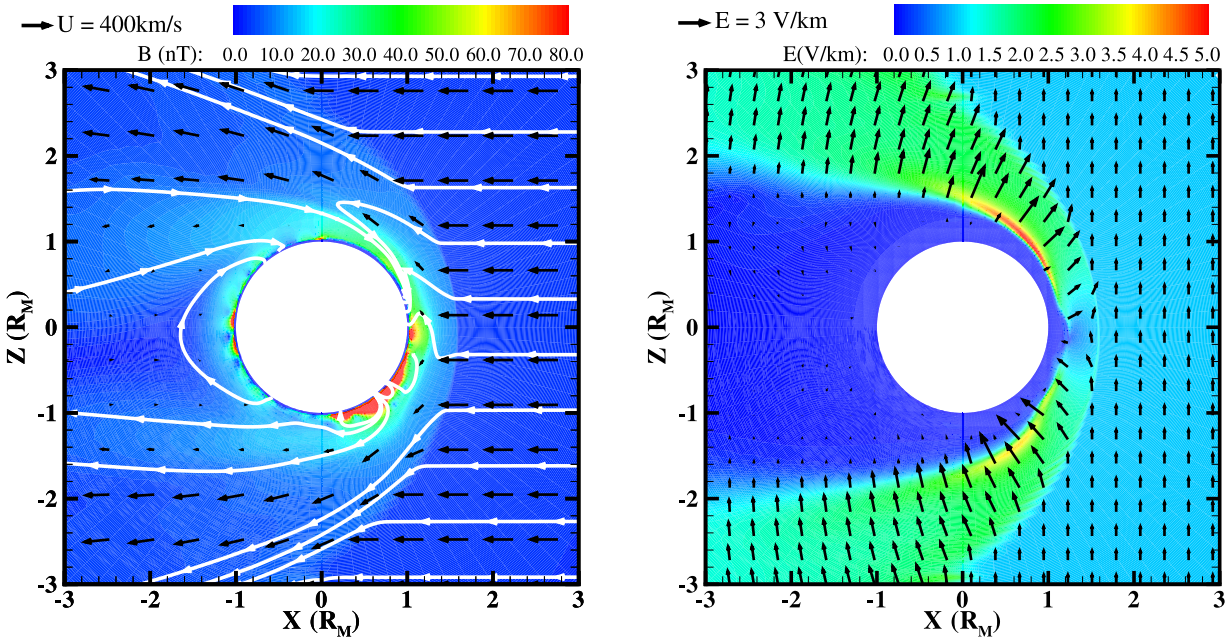

Figure 1. MHD simulation results for the plasma velocity, magnetic field and convection electric field in the *X*-*Z* plane. The color contours represent the magnitudes of (left) the magnetic field and (right) the electric field, respectively. The white lines marked with arrows in the left panel indicate the vector direction of the magnetic field. The black arrows indicate (left) the plasma bulk velocity and (right) the convection electric field, respectively.

by *Ma et al.* [2004]. In the photo-ionization calculation of the Martian atmosphere, the optical depth effect is taken into account by including a cosine factor for the solar zenith angle. The crustal magnetic field is added in the model by using the spherical harmonic crustal magnetic field model of *Arkani-Hamed* [2001]. The model has a spherical grid structure, allowing a radial resolution of around 10 km in the ionospheric region (~100 km altitude).

[13] In this study, the background Martian electromagnetic environment for the test particle modeling is taken from the MHD results for simulation case 1 by *Ma et al.* [2004]. In this case, the strongest crustal magnetic field position faced the Sun. The IMF was assumed to be a Parker spiral of 56° with a total field strength of 3 nT. The solar wind proton density was taken to be 4 cm^{-3} with the solar wind speed of 400 km s^{-1}. The Martian neutral atmosphere (with 3 species of CO_2, O, and H) was assumed to be spherically symmetric. The atmospheric densities, temperatures and photo-ionization frequencies were associated with solar maximum conditions.

[14] A Cartesian coordinate system is adopted, in which the *X* axis points from Mars to the Sun, the *Z* axis is perpendicular to *X* and parallel to the projection of the North Pole on a plane perpendicular to the *X* axis, and the *Y* axis completes a right handed orthogonal set (positive *Y* toward dusk). In our simulation case, the IMF is in the *X*–*Y* plane, and the solar wind velocity has only a negative *X* component. As a result, the convection electric field in the upstream solar wind, $\mathbf{E}_{sw}$, is oriented in the positive *Z* direction,

$$\mathbf{E}_{sw} = -\mathbf{U}_{sw} \times \mathbf{B}_{sw}, \quad (1)$$

where $\mathbf{U}_{sw}$ and $\mathbf{B}_{sw}$ are the flow velocity and magnetic field in the upstream solar wind, respectively. Given the fact that the actual orientation of the IMF varies frequently, another coordinate system, MSE (Mars-Sun-Electric field), is widely used for a better physical understanding of the Martian plasma environment. In the MSE reference frame, X_{MSE} points toward the Sun, Z_{MSE} coaligns with the interplanetary electric field plane (that is, $\mathbf{E}_{sw}$), and Y_{MSE} completes the right-hand system. It can be seen that the coordinate system adopted in the current simulation case is exactly aligned with MSE. In other words, the calculation results presented in this paper can be interpreted as being in the MSE coordinate system for a more meaningful understanding.

[15] Figure 1 shows the MHD simulation results for the plasma velocity, magnetic field and convection electric field in the *X*–*Z* plane. The electric field is defined as

$$\mathbf{E} = -\mathbf{U} \times \mathbf{B}, \quad (2)$$

where $\mathbf{U}$ is the bulk plasma velocity around Mars, $\mathbf{B}$ is the magnetic field. It is seen that the Martian obstacle (ionosphere and the crustal magnetic field) stands off the incoming solar wind plasma, creating the bow shock and the magnetic pile-up boundary (MPB). The MPB is the magnetospheric obstacle boundary which slows and deflects the solar wind. In the magnetosheath region bounded by the BS and MPB, the magnetic field compression results in the intensification of the convection electric field. It is notable that in the +*Z* magnetosheath region, the electric field has a sunward component. In contrast, it is slightly oriented tailward in the −*Z* region. Inside the MPB obstacle, the magnitudes of the plasma speed and thus the electric field

fall off sharply. This electromagnetic environment provides the background conditions within which the motion of test particles is determined.

2.2. The Test Particle Model

2.2.1. Test Particle Distribution

[16] We have developed a parallel 3-D Monte Carlo model that describes how Mars pickup oxygen ions are transported and accelerated once they are generated in the Martian oxygen corona. The neutral oxygen atmosphere consists of a thermal component and a hot component. Pickup oxygen ions can be generated from three mechanisms: (1) the ionization by the solar radiation, ($O + h\nu \rightarrow O^+ + e^-$); (2) the charge exchange collisions with ions ($O + H^+ \rightarrow O^+ + H$, $O + CO_2^+ \rightarrow O^+ + CO_2$); and (3) the impact ionization by solar wind electrons ($O + e^- \rightarrow O^+ + e^- + e^-$). The first two pickup ion sources are calculated using the rates given by *Ma et al.* [2004]. The solar wind electron impact ionization is calculated following *Cravens et al.* [1987]. The electron temperature is assumed to be half of the plasma temperature.

[17] In the test particle model, the source term grids are uniformly spaced with respect to the natural logarithm of the radial distance (300 km above the Mars surface up to 3 R_M, where R_M = 3396 km is the radius of Mars), resulting in a spatial resolution of approximately 37 km at the bottom and 101 km at the top. The inner boundary of the simulation domain at 300 km altitude is slightly above the Martian exobase, which was estimated to be around 215 km altitude for high solar cycle conditions [*Nagy et al.*, 2001]. The collisions of pickup ions with the ambient neutrals are thus reasonably neglected in this study. The grid spacing in the horizontal dimensions is 5° longitude by 5° latitude, making a total of 102 × 72 × 36 cells in the simulations. It is worth emphasizing that in the test particle model we report here as well as in the *Ma et al.* [2004] MHD model, a Cartesian coordinate system is adopted although a spherical grid structure is used.

[18] There are two ways to randomly distribute the starting points of test particles. One is to launch particles with an exponential falloff in the point density to mimic the neutral source. The other is to use a fixed number of test particles in each source cell. We adopt the second strategy in our test particle model for two reasons. First, as will be shown later, the test particles passing through a spatial location far away from Mars have their source regions at high altitudes, where the production rates are low. In other words, the statistical error for the fluxes coming from the tenuous upper atmosphere would be severe if the particle weighting favors low altitudes. Second, the particle number released in every single source cell in our model is sufficiently large to allow this approach, which is even larger than the total number in the whole simulation domain used in the study of *Kallio and Koskinen* [1999]. Unless specified explicitly, 10^4 test particles per source cell are launched in this study, giving 2.6×10^9 particles in the simulation domain in total.

[19] In a source cell volume, the starting points of test particles are uniformly distributed in space. Each test particle carries a weight to normalize the initial test particle distribution to match the real pickup ion population around Mars. The weight, which is the same for all the particles originating in a source cell, is defined as the total pickup ion production per unit time in that cell divided by the number of the test particles. The velocity distribution for a new-born particle is assumed to be isotropic and Maxwellian, with the temperature equal to that of the local neutral atmosphere.

2.2.2. Pickup Ion Transport

[20] Pickup ion transport around Mars is governed by the Lorentz force within the magnetic field and convection electric field. The motion of a single charged ion is followed by solving Newton's equations,

$$\frac{d\mathbf{r}}{dt} = \mathbf{v}, \tag{3}$$

$$\frac{d\mathbf{v}}{dt} = \frac{e}{m}(\mathbf{E} + \mathbf{v} \times \mathbf{B}), \tag{4}$$

where $\mathbf{r}$ and $\mathbf{v}$ are the location and velocity of a particle, respectively. e is the electric charge. $\mathbf{B}$ and $\mathbf{E}$ are the magnetic and electric fields, respectively, at the location of the particle. $\mathbf{B}$ is calculated in the 3-D MHD simulation case 1 of *Ma et al.* [2004]. $\mathbf{E}$ is given by equation (2). The 3-D MHD simulation results therefore provide the background Martian electromagnetic conditions for our test particle simulation.

[21] The numerical solution of Newton's equations is performed using a staggered leapfrog scheme. The discretized equations are

$$\frac{\mathbf{r}^{n+1} - \mathbf{r}^n}{\Delta t} = \mathbf{v}^{n+\frac{1}{2}}, \tag{5}$$

$$\frac{\mathbf{v}^{n+\frac{1}{2}} - \mathbf{v}^{n-\frac{1}{2}}}{\Delta t} = \frac{e}{m}\left(\mathbf{E}^n + \frac{\mathbf{v}^{n+\frac{1}{2}} + \mathbf{v}^{n-\frac{1}{2}}}{2} \times \mathbf{B}^n\right), \tag{6}$$

where Δt is the simulation time step (0.05 sec), n denotes the time level. The spatial location (and thus the magnetic and electric fields) and the velocity are evaluated at alternating half time steps, as seen in equations (5) and (6).

[22] The time advancing of the velocity vector (from a previous time $(n - \frac{1}{2})\Delta t$ to the new time $(n + \frac{1}{2})\Delta t$) is carried out using the Boris scheme [*Birdsall and Langdon*, 1985]. The electric and magnetic forces are separated by introducing two new velocity vectors,

$$\mathbf{v}^- = \mathbf{v}^{n-\frac{1}{2}} + \frac{\Delta t}{2}\frac{e}{m}\mathbf{E}^n, \tag{7}$$

$$\mathbf{v}^+ = \mathbf{v}^{n+\frac{1}{2}} - \frac{\Delta t}{2}\frac{e}{m}\mathbf{E}^n, \tag{8}$$

leading to

$$\mathbf{v}^+ - \mathbf{v}^- = \frac{\Delta t}{2}\frac{e}{m}(\mathbf{v}^+ + \mathbf{v}^-) \times \mathbf{B}. \tag{9}$$

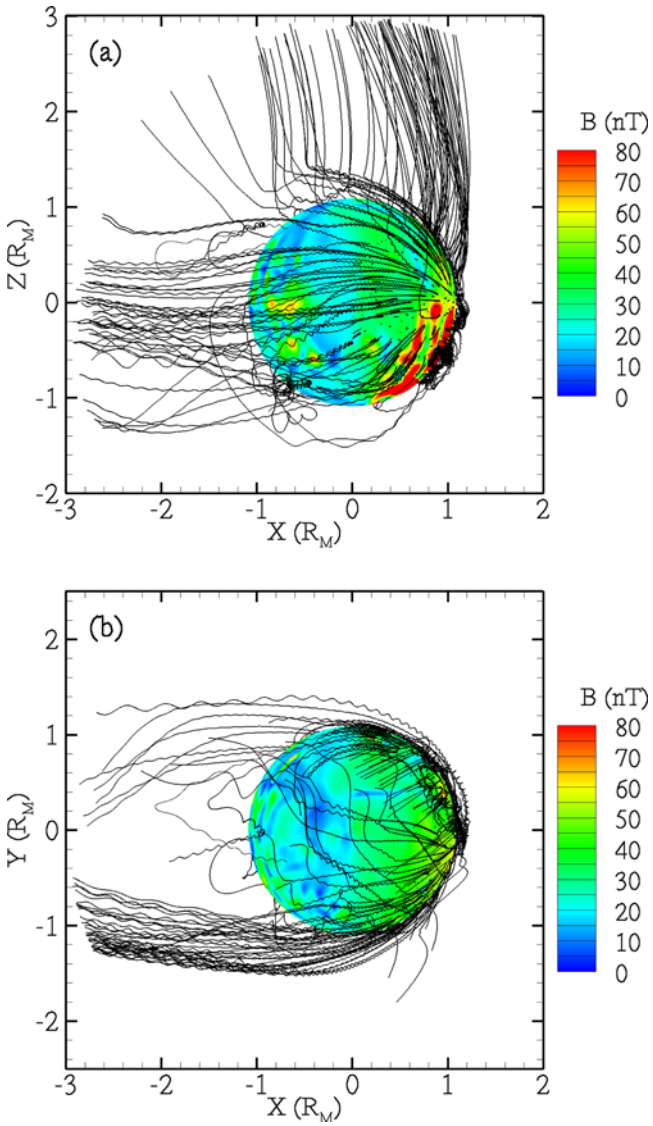

Figure 2. Sample pickup O^+ trajectories projected (a) in the *X*-*Z* plane, and (b) in the *X*-*Y* plane. The color represents the magnitude of the magnetic field at 300 km altitude above the Martian surface.

The transformation from $\mathbf{v}^-$ to $\mathbf{v}^+$ is a rotation about $\mathbf{B}$ with an angle α, which is given by

$$\tan\frac{\alpha}{2} = \frac{|\mathbf{v}_\perp^+ - \mathbf{v}_\perp^-|}{|\mathbf{v}_\perp^+ + \mathbf{v}_\perp^-|} = \frac{\Delta t}{2}\frac{e}{m}|\mathbf{B}|. \tag{10}$$

Therefore the acceleration of a particle in equation (6) is broken into three steps: (1) a half step of electric acceleration (from $\mathbf{v}^{n-\frac{1}{2}}$ to $\mathbf{v}^-$ in equation (7)); (2) a rotation in the plane perpendicular to the magnetic field (from $\mathbf{v}^-$ to $\mathbf{v}^+$ in equation (9)); and (3) a half step of electric acceleration (from $\mathbf{v}^+$ to $\mathbf{v}^{n+\frac{1}{2}}$ in equation (8)).

[23] The motion of an ion within the magnetic and electric fields is a cycloid, which is a superposition of a gyration around local magnetic field lines and an $\mathbf{E} \times \mathbf{B}$ drift. Because of the lack of a strong intrinsic magnetic field, the gyroradius can be comparable to or even larger than the planetary scale, making the kinetic effect prominent. In the model, a test particle is traced in the computational domain. Particles are removed from the simulation whenever they impact at the inner spherical boundary (300 km above the Martian surface) or escape from the outer boundary (3 R_M from the center of the planet). By recording the spatial and velocity information of a large number of representative test particles, we can investigate the pickup ion flux distribution around Mars.

[24] Figure 2 shows the projection of sample pickup O^+ trajectories in the noon-midnight and equatorial planes. This provides an overall picture of how Mars interacts with the solar wind in the view of the pickup ion distribution. A reasonably small number of test particles are launched to make the plots easier to view, but are still sufficient to illustrate the global ion distribution. A total of 733 test particles are released to trace out the full pickup ion generation. Instead of using a fixed number of test particles in a source cell (which is the strategy we use to produce all the other simulation results in this paper), the initial point density is proportional to the local pickup ion production rate. The transport of the sampled test particles that are distributed in this way actually represents the global pickup ion population.

[25] As seen in Figure 2, the pickup ions are basically characterized into three major groups. One group of particles originate close to or within the magnetosheath region. When the particles are in the magnetosheath, they are easily accelerated to high energy owing to the strong electric field there (see Figure 1). As a result, the ion gyroradius is of the same order as the planetary size. The particles move toward the $+Z_{MSE}$ direction, forming the polar plume. Another group of pickup ions are generated inside the MPB and have small gyroradii due to the extremely weak electric field and the relatively strong magnetic field. They pass through the flank sides of Mars and slightly merge toward the *X* axis in the tail region. The other group of pickup ions crash back into the atmosphere of the planet, constituting a precipitating energy flux to the dayside Martian atmosphere [*Luhmann and Kozyra*, 1991].

[26] The kinetic effects of pickup ions at finite gyration are well demonstrated in the asymmetric distribution in Figure 2. The $+Z_{MSE}$ component of the convection electric field, which is due to the $+Y_{MSE}$ component of the IMF in the simulation, transports particles outside of the computational domain over the north pole region. In addition to the north-south direction, there is also a notable dawn-dusk asymmetry in the particle distribution. The Parker spiral magnetic field configuration in the incoming solar wind makes the $\mathbf{E} \times \mathbf{B}$ drift have a $-Y_{MSE}$ component on the dayside. This explains the reason why the particles on the duskside flank are more easily lost by impacting the Martian atmosphere. As a consequence, the tail ray on the dawnside is much stronger than that on the duskside.

2.2.3. Parallelization

[27] In our model, more than 10^9 test particles in total are employed to allow unprecedented examination of the velocity space distribution at various spatial locations around Mars. Therefore the code has been written for parallel computing on a multiprocessor machine. A master-slave communication structure is used to facilitate the parallelization. At the beginning, only the master processor is assigned

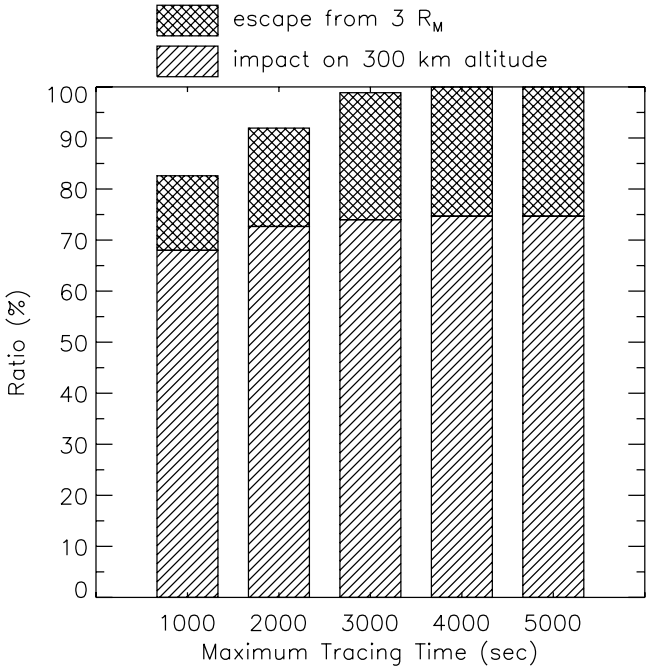

Figure 3. Partition of test particles that ultimately precipitate at the inner boundary or escape from the outer boundary. The ratios are shown with respect to different maximum times used in the particle tracing.

the whole work, while all the slave processors are idle. As time proceeds, the work of test particle tracing is distributed to the slave processors upon their request.

[28] To minimize processor idle time, an efficient form of dynamic load balancing is required to maintain equity among processors. In dynamic load balancing, when a processor runs out of work, it can request additional work from other processors. To make use of system resources as far as possible, one slave processor not only can perform the work that is assigned by the master processor, but also can ask for a job from other slave processors. Furthermore, when the master processor is free of work, it can also make a request from the slave processors. The dynamic work distribution may introduce some communication overhead for work requests and message transfer. However, the algorithm efficiently reduces load imbalance among the processors. Speedup is therefore achieved in general.

2.2.4. Tracing Time Convergence

[29] In the model, a test particle originates within the simulation domain and is continuously monitored until the inner or the outer boundary is reached. In practice, a limitation is imposed on the maximum tracing time of particle transport. Figure 3 presents the partition ratios of test particles that ultimately crash back into the atmosphere or escape out of the simulation domain. Different maximum tracing times are applied to compare the results. It is found that more than 8% of the test particles still stay in the interior of the domain when the maximum tracing time is shorter than or equal to 2000 s. This is because some particles inside of the MPB (where the convection electric field is extremely weak) cannot obtain enough acceleration to make a long transport away from their starting locations. As the maximum time interval increases to more than 4000 s, all the test particles can transport out of the simulation domain. In this study, the maximum tracing time interval is set to be t_{max} = 3000 s. Two reasons are worth mentioning concerning this choice. First, the percentage of the very low energy test particles which cannot reach the domain boundaries becomes only 1% when t_{max} = 3000 s. These particles can be easily lost through the collisions with the local Martian corona, although the collisional effect is neglected in this work. Second, the maximum tracing time value is selected to avoid excessive computational effort on these local particles.

2.2.5. Escape Rate Convergence

[30] Figure 4 compares the total impact and escape rates of pickup O^+ ions when different number of test particles are launched in a source cell. The maximum particle tracing time of 3000 s is used here and throughout the paper. In this comparison, the particle number per source cell changes by three orders of magnitude from 10 to 10^4, resulting in the change of the total number in the whole simulation domain from 2.6×10^6 to 2.6×10^9, respectively. It is seen that increasing the total test particle number above one million essentially does not affect the impact and escape rates. For example, the total escape rates are constant at 3.7×10^{24} s^{-1}. Note that the pickup ion source term from electron impact ionization is not included in the MHD study of *Ma et al.* [2004]. The escape rate after the subtraction of the electron impact ionization source becomes 2.8×10^{24} s^{-1} in our test particle model, comparable to the MHD escape rate of 2.7×10^{24} s^{-1} through the r = 3 R_M surface. It is notable that the escape rate reported by *Ma et al.* [2004] was obtained by integrating tailward moving fluxes through a $X = -10$ R_M plane with dimensions -16 $R_M \leq Y, Z \leq 16$ R_M. It is important to point out that the escape fluxes calculated by the MHD model also include escaping ions from the Martian

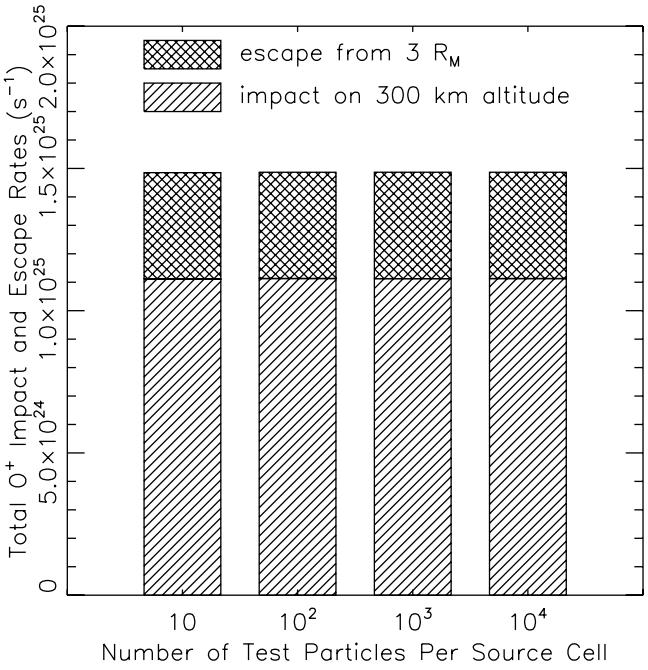

Figure 4. Total impact and escape rates of pickup oxygen ions. The results are presented for the different number of test particles launched per source cell in the simulations.

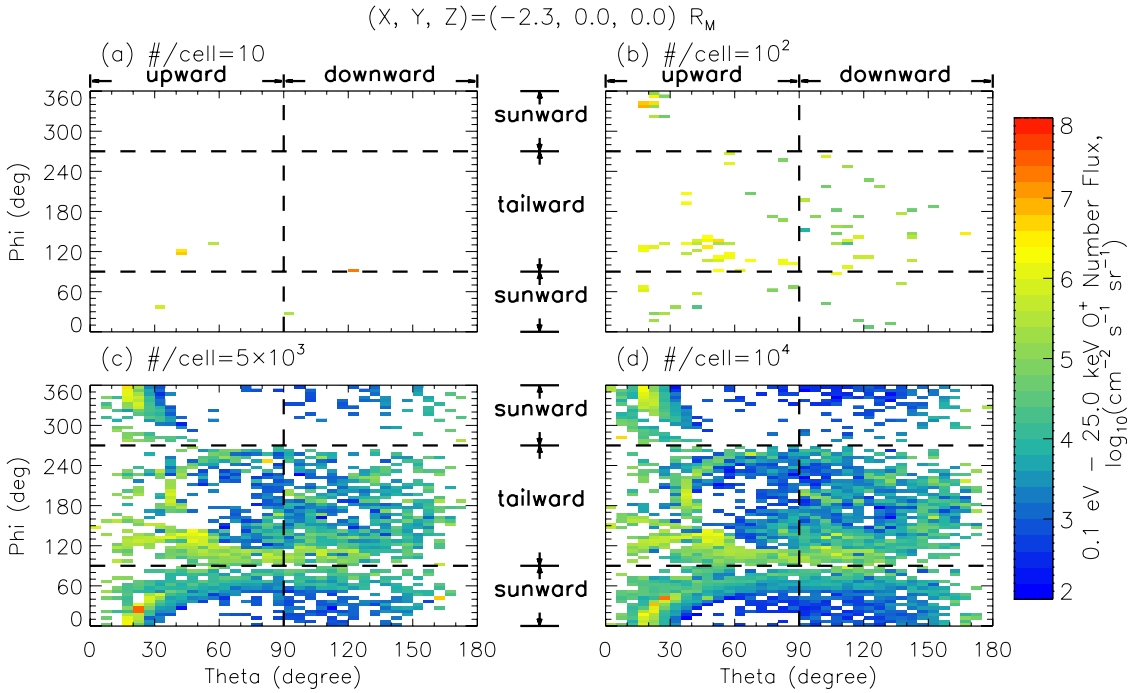

Figure 5. Velocity space distributions of pickup O^+ ions at a distance of 2.3 R_M down the tail. The results are shown with respect to different numbers of test particles per source cell in the simulations: (a) 10, (b) 10^2, (c) 5×10^3, and (d) 10^4.

ionosphere; that is, from beneath the inner boundary of our simulation domain (300 km altitude). These escaping ionospheric ions are estimated to increase the total flux up to about a factor of 2 [*Ma and Nagy*, 2007].

[31] Because of different solar wind conditions and Martian atmospheric profiles used in different model set ups, it is hard to make a quantitative comparison of the O^+ escape rate. The previously estimated escape rate ranges from 10^{23} s^{-1} to 3×10^{25} s^{-1}, either by satellite measurements [*Lundin et al.*, 1990; *Verigin et al.*, 1991; *Barabash et al.*, 2007], or by various models [*Luhmann*, 1990, 1997; *Zhang et al.*, 1993; *Kallio and Koskinen*, 1999; *Ma et al.*, 2004; *Modolo et al.*, 2005]. It is seen that our calculated pickup O^+ escape rate falls well within the bounds of the aforementioned estimates in the literature, validating our test particle model. Since the electromagnetic fields of the *Ma et al.* [2004] model are applied as the background conditions for the particle transport in this study, it is interesting to compare our test particle model with their MHD model. While the two escape rate results are in close agreement, the difference between the models is worth being emphasized. The most distinguishing limitation with MHD results is the absence of the kinetic effects associated with large ion gyroradii. As constrained by the bow shock, the MHD fluids on the dayside are deflected toward the tail. However, our test particle simulation illustrates a different scenario. As shown in Figure 2, a prominent polar plume is formed, passing through the bow shock and constituting an important ion loss channel. Considering that the pickup ion escape is critical to understanding the long-term planetary atmosphere evolution, the spatial distribution of escaping ions deserves a more detailed investigation. A comprehensive comparison of the ion escape between the tail and polar loss channels is in progress, and will be published elsewhere.

2.2.6. Velocity Distribution Convergence

[32] In this section, the necessity of using an extremely large number of test particles in the simulations is investigated. It has been demonstrated that 10^6 test particles in total are sufficient to analyze the total pickup ion impact and escape rates. Let us proceed with an analysis of the influence of the number of test particles on the resolution of the particle velocity space distribution. To resolve the pickup ion flux distribution in velocity space, all the particles passing through a spatial location (a pseudo-detector) are recorded with the energy and angular information. There are 68 energy bins, equally spaced in the natural logarithmic scale from 0.1 eV to 25 keV. Two angular coordinates (θ, ϕ) are defined to represent the velocity direction. The coordinate θ is the polar angle, which is the angle of the particle moving direction measured from the $+Z$ axis. So, when $0° < \theta < 90°(90° < \theta < 180°)$, the velocity of a particle has a $+Z(-Z)$ component. The coordinate ϕ is the azimuthal angle from the $+X$ axis in the X-Y plane. That is, a particle of $90° < \phi < 270°$ has a tailward moving direction. The other ϕ values correspond to a sunward moving. The angular grid spacing is specified to be 5° in θ by 5° in ϕ. To improve the statistics, the collection area at a point, which is oriented along the X axis, has a circular cross section of radius 30 km. This distance is so sufficiently short (<0.01 R_M) that the change of the flux distribution in this scale can be reasonably neglected.

[33] Figure 5 presents the results of the convergence test for the velocity space distribution at the point of $X = -2.3$ R_M down the tail as an example. Numerical experi-

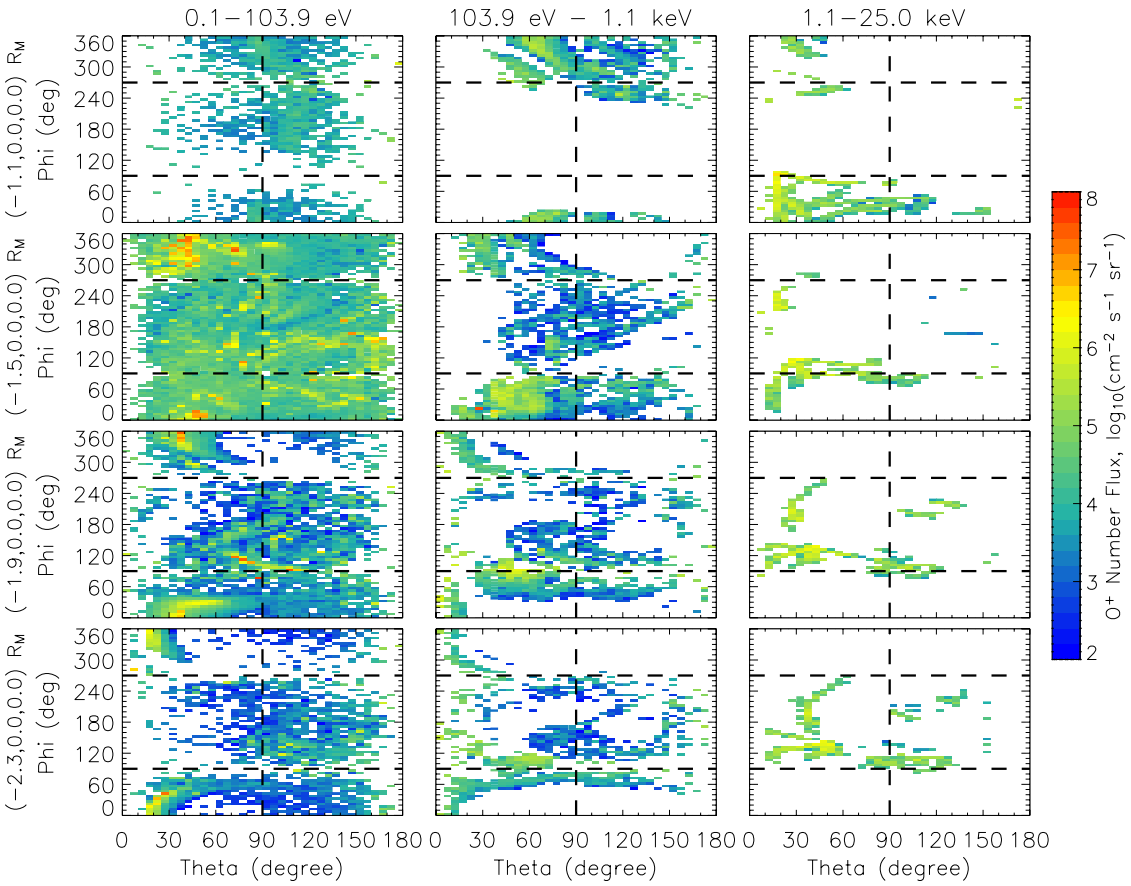

Figure 6. Velocity space distributions of pickup O^+ fluxes passing through various spatial points along the tail: $X = -1.1$, -1.5, -1.9, and -2.3 R_M (4 rows). The fluxes are given in low, medium, and high energy channels (3 columns). The color coding is in a logarithmic (base 10) scale.

ments are performed to test the sensitivity of the flux distribution resolution to the number of test particles used in the simulations. The particle number per source cell changes by three orders of magnitude from 10 to 10^4. It is clearly shown that the simulation with 10 particles per cell only generates very sparse data points. The data point density is greatly enhanced when 10^2 test particles are launched in a cell, but still insufficient for an acceptable resolution level. When the number further increases by two orders of magnitude, the data points tend to reach a saturation. This convergence is evident by comparing the velocity space distribution plots for particle number 5×10^3 and 10^4 per cell. Therefore we can draw a conclusion that a total of 10^6 test particles (Figure 5a), which were used in previous studies, are far from enough to resolve the pickup ion velocity space distribution around Mars, although they are sufficient to estimate the total impact and escape rates. Instead, 10^4 test particles per cell (corresponding to more than 10^9 in total) are favored for a reasonably high resolution, which are employed in our current test particle model.

3. Results

[34] In the previous section, we have shown the velocity space distribution results for the pickup ion fluxes in the Martian tail region. It is well illustrated that the velocity space distribution is highly non-Maxwellian, exhibiting many beam-like features. However, more emphasis was placed on the justification for the necessity of using more than 10^9 test particles in the model. Here, more detailed results at a variety of locations along the tail are provided. It will be shown that the velocity space distribution information can be used as a diagnostic tool for understanding the Mars-solar wind interaction.

[35] Figure 6 presents the velocity space distributions of pickup O^+ ions at various spatial locations along the tail. The pseudo-detectors are spaced from $X = -1.1$ R_M to $X = -2.3$ R_M at every 0.4 R_M. Like in Figure 5, the values of $\theta = 90°$, $\phi = 90°$ and 270° are marked to help indicate the particle moving direction, whether tailward or sunward, upward (having $+Z$ component) or downward (having $-Z$ component). The bottom panels of Figure 6 are similar to Figure 5d, but broken into low (0.1−103.9 eV), medium (103.9 eV−1.1 keV), and high (1.1−25 keV) energy channels.

[36] One prominent feature in Figure 6 is the pickup ion outflow in the tail region. This tailward motion is well studied with satellite measurements [*Lundin et al.*, 1990; *Kallio et al.*, 1995] and models [e.g., *Kallio and Koskinen*, 1999; *Kallio and Janhunen*, 2002; *Ma et al.*, 2004]. As illustrated by our test particle model, the tailward flow manifests itself in the whole energy range, particularly in the high energy channel. However, there are two exceptions

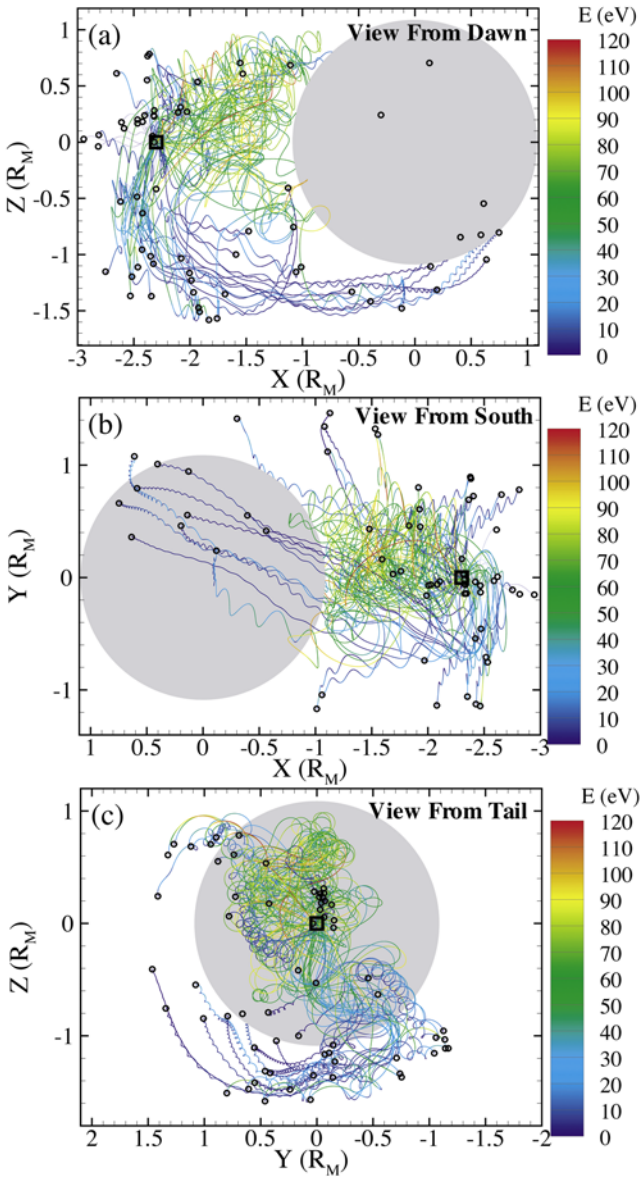

Figure 7. Sample trajectories of pickup O^+ passing through a spatial point of $(X, Y, Z) = (-2.3, 0, 0)$ R_M with energies below 103.9 eV. The location of the pseudo-detector is marked by the open square. Open circles indicate the starting locations of the particles. The moving paths are color-coded by the particle energies. The views are made from (a) dawn, (b) south, and (c) tail, respectively.

to this outflow. One exception occurs fairly close to the planet. It is readily seen in the medium and high energy channels of the $X = -1.1$ R_M pseudo-detector that the particle fluxes are more focused on the sunward moving direction. This anti-tailward $\mathbf{E} \times \mathbf{B}$ drift results from the sunward plasma flow at low altitudes by the MHD model [see Figures 3 and 4 by *Ma et al.*, 2004]. The other exception to the tailward outflow takes place when particle energies are relatively low, for example, $X \leq -1.9$ R_M with energy lower than 1 keV. However, it is notable that these particle streams have more of an upward moving direction ($\theta \leq 30°$) than a sunward direction.

[37] For a better understanding of the velocity space distributions, Figure 7 presents the sample trajectories of pickup O^+ passing through $X = -2.3$ R_M in the tail with energies below 103.9 eV. This figure is in correspondence with the lower left panel of Figure 6. As seen in Figure 6, the particles hitting the pseudo-detector can be characterized into two major groups: (1) upward and sunward moving

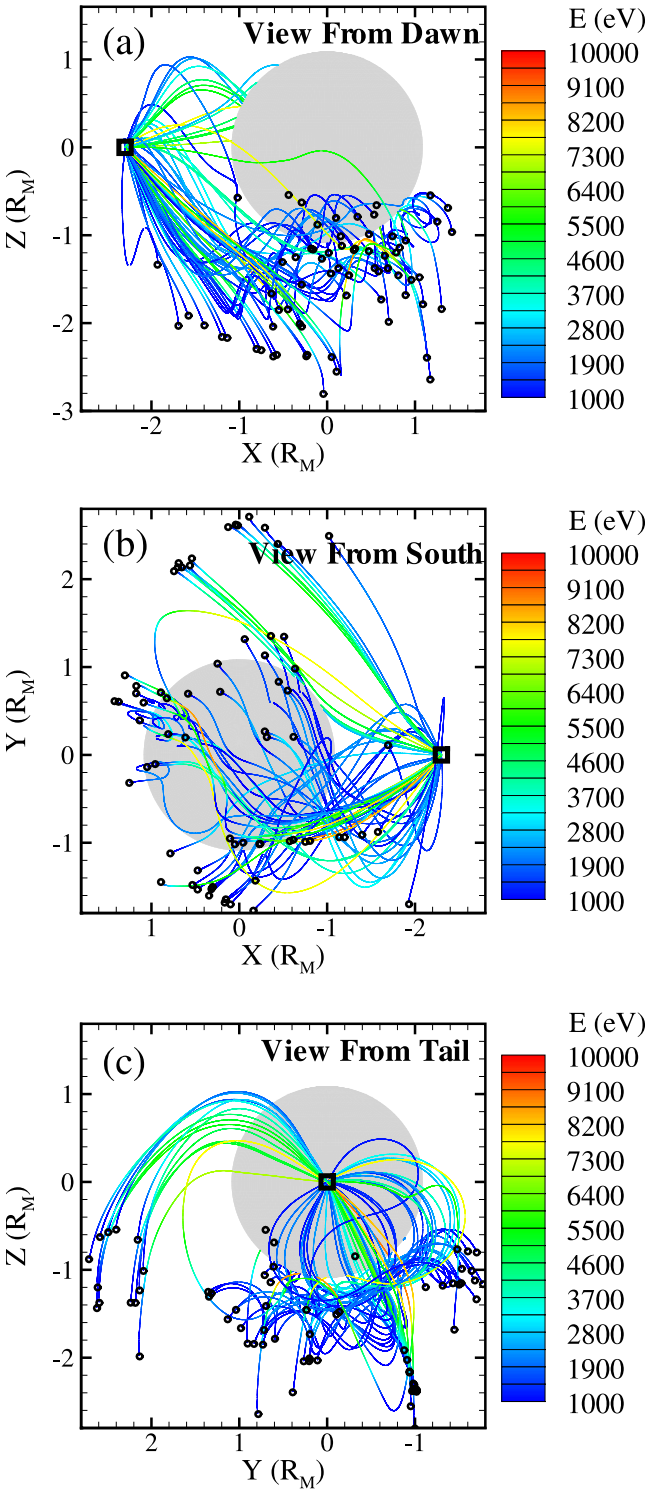

Figure 8. Similar to Figure 7 but for energy higher than 1.1 keV.

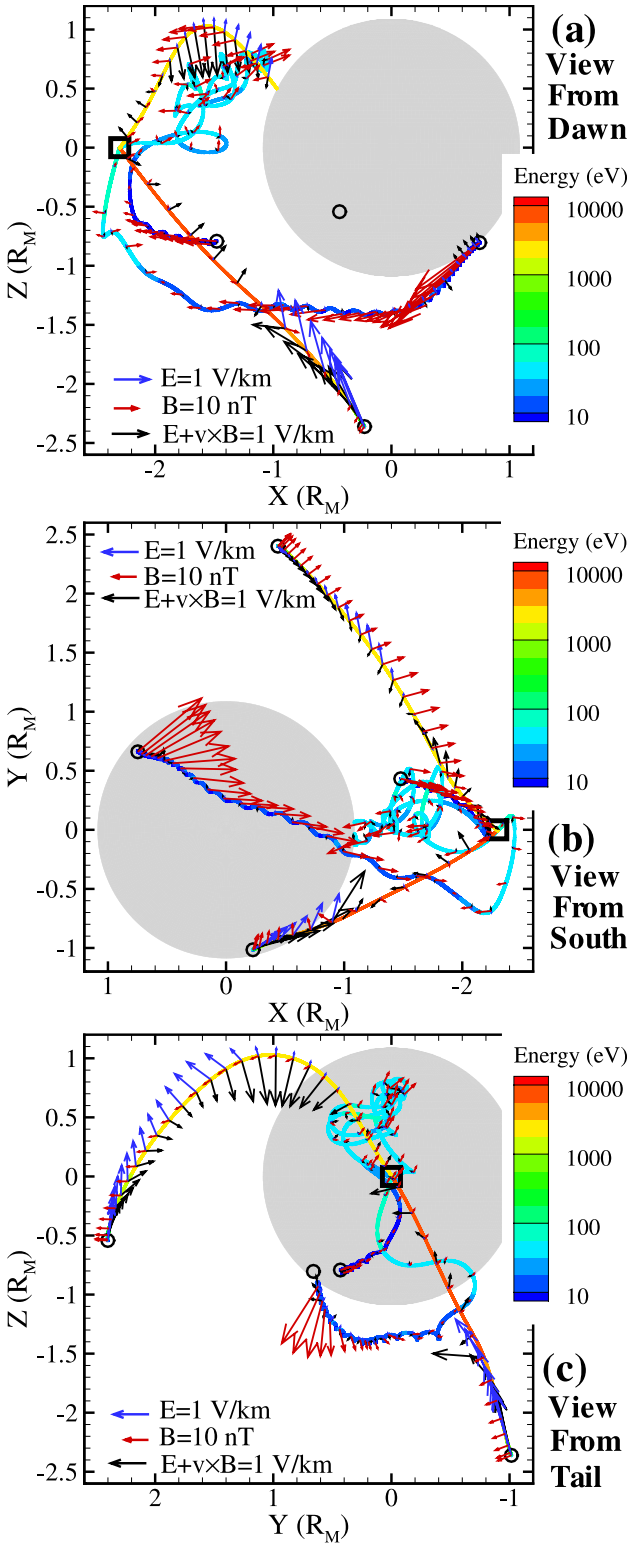

Figure 9. Magnetic field, convection electric field, and Lorentz force ($\mathbf{E} + \mathbf{v} \times \mathbf{B}$) along four sample particle trajectories. These field vectors (including direction and magnitude) are indicated by red, blue and black arrows, respectively. The moving paths are color-coded by the energies on a logarithmic scale. The symbols of open circles and squares have the same meaning as in Figure 7. The views are made from (a) dawn, (b) south, and (c) tail, respectively.

particles (the yellow-red shading in the lower left and upper left corners of the panel), and (2) tailward and downward moving particles (the blue-green shading in the middle right side). The originating locations and the cycloidal trajectores of these particle groups are demonstrated in Figure 7. Since their main activity domain is inside the MPB where the convection **E** field is extremely weak, the particles obtain no significant acceleration and their flight paths are deflected mostly by the **B** field. The trajectories are thus interwoven in a complicated way. The particles originating in the southern hemisphere ($-Z_{MSE}$) can travel upward through the pseudo-detector or curve deep into the optical shadow region and then hit the detector in a tailward direction after a number of gyrations.

[38] Similar to Figure 7, the sample trajectories of particles that hit the $X = -2.3$ R_M pseudo-detector within a high energy range (>1.1 keV) are shown in Figure 8. They are representative of the distribution plot in the lower right corner of Figure 6. Different from the particles in Figure 7, the high energy particles in Figure 8 originate in the magnetosheath region, where the **E** field is strong (see Figure 1). As a result, the particles are efficiently accelerated to high energies. With a faster speed, their gyroradii are significantly larger than those in Figure 7. It is seen that the high energy particles crossing through the spatial location far down the tail mostly have their source region in the southern hemisphere. Some particles generated on the duskside flank can also travel and contribute to the incidenting flux, in the downward and dawnward direction.

[39] Figure 9 shows the magnetic field, convection electric field, and Lorentz force ($\mathbf{E} + \mathbf{v} \times \mathbf{B}$) along four sample particle trajectories. Two of the particles are from Figure 7; that is, their impacting energy at the pseudo-detector at $X = -2.3$ R_M is lower than 103.9 eV. One has an upward and sunward moving direction passing through the spatial location, while the other has a tailward and downward direction. The other two of the particles are selected from Figure 8 with the energies higher than 1.1 keV. One originates in the southern hemisphere, while the other comes from the duskside flank. The **B**, **E** and Lorentz force vectors are superposed on the cycloidal trajectories to understand the particle motion. The electromagnetic fields are specified using the MHD model results of *Ma et al.* [2004] (see Figure 1 for the big picture of the **B** and **E** fields in the computational domain). It is clearly shown in Figure 9 that the difference in the acceleration highly depends on where the particles come from. Particles that originate inside the MPB encounter an extremely weak convection electric field (indicated by very short blue arrows) and their motion is essentially controlled by the magnetic field. In contrast, the particles generated in the magnetosheath region are easily accelerated to a high energy, where the stronger electric field is indicated by long blue arrows. After entering the magnetosphere, the motion of the particles are deflected by the magnetic field therein. The complicated **B** and **E** field configurations around Mars give rise to the complexity of the pickup ion flux distribution.

4. Discussion

[40] Figures 6 to 9 demonstrate that the pickup O^+ ion distribution in velocity space carries important information

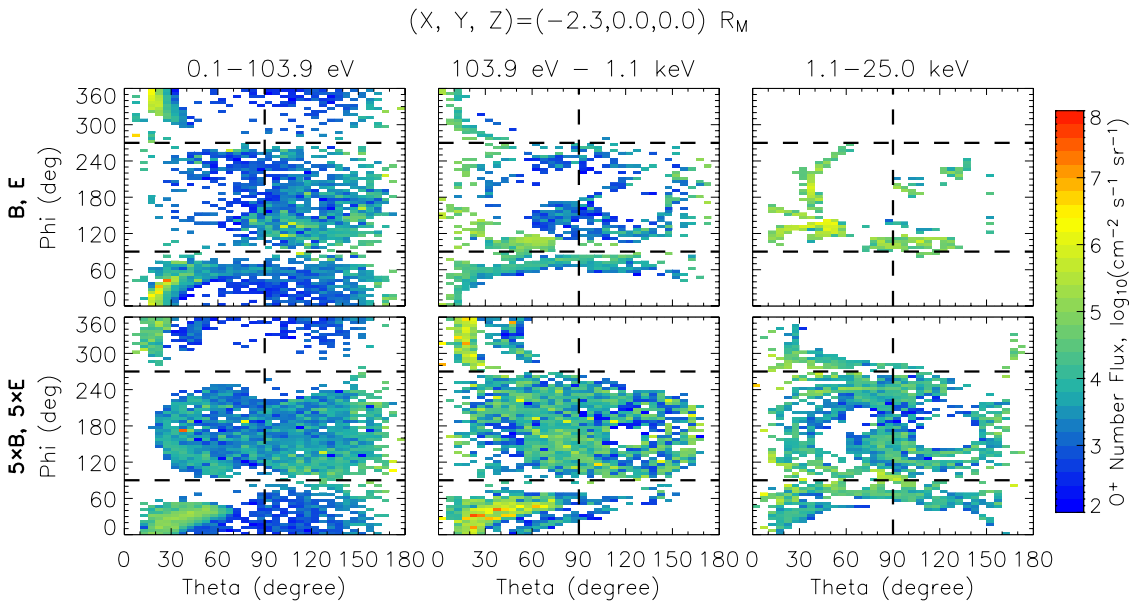

Figure 10. Comparison of the velocity space distributions of particles passing through $X = -2.3$ R_M in the tail between (top) a baseline case and (bottom) an active case. In the active case, the **B** and **E** fields are artificially intensified by a factor of 5. The plot format is the same as in Figure 6.

about the planetary atmospheric escape. Trajectory tracing in a reverse direction is capable of locating the source regions of particles passing through any spatial point. Given the fact that the particle transport is strongly affected by the electromagnetic environment, the velocity space distribution can thus be used as a unique tool to probe the Mars-solar wind interaction.

[41] To illustrate how the velocity space distribution is reflective of the Mars-solar wind interaction, two cases are compared side by side in Figure 10. A pseudo-detector is placed at $(X, Y, Z) = (-2.3, 0, 0)$ R_M. In a baseline case, the **B** and **E** fields are the same as we have used in this study. For the comparison purpose, the bottom panels of Figure 6 have been repeated in Figure 10. In an active case, both of the **B** and **E** fields are artificially intensified by a factor of 5, while the rest of the parameters remain unchanged. It is notable that the electromagnetic fields in the active case are not self-consistently coupled with the plasma flow any more. However, this active case somewhat represents a solar wind condition with a 5× intensified IMF and an unchanged velocity (see equation (2)). Considering that Mars is an unmagnetized planet, the interaction structure is more affected by the solar wind speed. We must also be careful that this simplified numerical experiment actually increases the planetary magnetic field at the same time, although there is no well-established knowledge on the impact of that on the whole picture of the Mars-solar wind interaction. However, it is useful to see what difference it makes in the pickup ion velocity space distribution by simply changing the **B** and **E** fields.

[42] The comparison in Figure 10 clearly shows the dependence of the pickup ion velocity space distribution on the Mars-solar wind interaction conditions. As **B** and **E** are intensified, more particles are observed in the medium and high energy channels far down the tail. This is understandable, as the intensification of the electric field effectively broadens the source region where new-born pickup ions can obtain a significant acceleration. Another noteworthy feature is that particles with a sunward moving direction begin to appear in the high energy channel. In reality, the change with respect to varying solar wind and solar radiation conditions is more complicated than what is presented here in a simplified active case. However, it is well demonstrated in Figure 10 that the velocity space distribution information of pickup ions is sensitive to the electromagnetic fields and thus can be used to infer the Mars-solar wind interaction.

[43] It is hard to make a quantitative comparison among various test particle models due to differences in a number of aspects. For example, the global electromagnetic environment used in the models are quite different. In the early models, the background **B** and **E** fields were obtained either using a gas dynamic approximation [*Luhmann and Schwingenschuh*, 1990; *Luhmann*, 1990; *Lichtenegger et al.*, 1995; *Lichtenegger and Dubinin*, 1998], or based on an empirical model [*Kallio and Koskinen*, 1999]. These highly simplified models lack the capability of self-consistently solving the **B** and **E** fields. In the previous studies, photoionization is considered as the only ionization source. In addition, the background atmospheric profiles as well as the computational domains are not the same. Therefore these differences prevent any direct comparison among the models. More importantly, all the existing models cannot accurately resolve the velocity space distribution of pickup ions, because an inadequate number of test particles were launched in their simulations.

[44] It should be noted that the test particle source region in our current model extends out to 3 Martian radii. It was illustrated by *Cravens et al.* [2002] that oxygen ions born at greater distances can significantly contribute to the higher energy parts of the velocity space distribution, that is, the 1.1−25 keV parts as shown in Figures 6 and 10. This is

because of the large gyroradii of oxygen ions picked up in the unshocked solar wind.

[45] The effect of the Martian crustal magnetic field has been added in the simulations reported here (see Figure 1). It was illustrated by *Ma et al.* [2004] and *Ma and Nagy* [2007] that the orientation of the magnetic anomaly regions has a significant effect on the bow shock standoff location and escaping particle fluxes. It is thus of particular interest to see how large this effect may be on the pickup ion distribution in velocity space. A systematic analysis of the pickup ion responses to a variety of crustal magnetic field orientation conditions is expected to provide key information to understand the role of magnetic anomalies in the particle distribution. Such simulations and comparison are planned for a future investigation.

[46] With the unprecedented capability of resolving the pickup ion velocity space distribution, our simulation results can be used to better understand in situ measurements of the ion mass analyzer (IMA) of the ASPERA-3 instrument suite onboard the Mars Express satellite [*Lundin and Barabash*, 2004]. By setting appropriate solar wind and Martian atmospheric conditions in the 3-D MHD model [*Ma et al.*, 2004], we can run our test particle model in a more realistic electromagnetic environment and attempt to reproduce IMA observations. The data-model comparison undoubtedly will enhance our understanding of the Mars-solar wind interaction. However, this paper aims to introduce a new research tool that combines two sophisticated 3-D models: a MHD model and a test particle model. In accordance with this purpose, the present paper is focused on the potential of probing Mars-solar wind interaction processes using the pickup ion distribution in velocity space rather than on the interpretation of existing satellite measurements. To interpret satellite data such as IMA, more extensive simulations of both the MHD model and the test particle model are required to incorporate realistic conditions, considering for example the solar wind plasma and IMF, the crustal magnetic field orientation, and solar cycles. The data-model comparison is beyond the scope of this study and should be an interesting topic of a future study.

[47] It is worth noting that the limitation of test particle models mainly comes from the fact that the magnetic and electric fields are not self-consistently calculated. The feedback of the electric currents carried by moving ions to the electromagnetic environment is neglected. A more rigorous approach is to create a hybrid system, where ions are still treated kinetically but electrons are considered as a massless fluid [*Brecht et al.*, 1993; *Brecht*, 1997; *Kallio and Janhunen*, 2002; *Modolo et al.*, 2005]. By this means, particle motion is self-consistently coupled with the electromagnetic fields. However, due to the limitation on available computational sources, the spatial and energy resolutions of existing hybrid models are far from being satisfying. Our test particle model is the only one at present that is capable of providing a high resolution pickup ion distribution in full velocity space.

5. Summary and Conclusion

[48] In this paper, we report a newly created highly parallelized global test particle model for resolving the velocity space distribution of pickup O^+ ions around Mars. There are a number of novel features about this model. First, a state-of-the-art 3-D multispecies MHD model [*Ma et al.*, 2004] is employed to provide the background Martian electromagnetic environment, within which the pickup ion transport is traced. The magnetic and electric fields are self-consistently solved together with the plasma flow around Mars. Second, a number of pickup ion sources are considered. In most existing test particle models, photo-ionization is the only mechanism considered for pickup ion production. In addition to photo-ionization, the pickup ion generation resulting from charge exchange and solar wind electron impact ionization is considered in this study as well. Finally and most importantly, more than 10^9 test particles are launched in our model. This corresponds to a major enhancement, by at least 3 orders of magnitude, in the total number of particles used, compared to all the existing test particle models. This substantial improvement provides an excellent opportunity to examine the pickup ion flux distribution in velocity space. A much smaller number of test particles used in previous models are adequate to estimate of the pickup ion distribution with respect to spatial locations. However, our numerical experiments evidently show that their test particle numbers fail to simulate the velocity space distribution at a spatial location. In this paper, the velocity space information of pickup ions is applied as a diagnostic tool to probe the Mars-solar wind interaction.

[49] In the tail region, pickup ions have a prominent outflowing component in the whole energy range. There are two exceptions to this outflow. One exception occurs fairly close to the planet, where the anti-tailward drift is consistent with the MHD results [*Ma et al.*, 2004]. The other exception happens far down the tail in a relatively low energy channel. However, the particle streams have more of an upward ($+Z_{MSE}$) direction than a sunward direction. The energy examination of particles traveling across the tail region shows that the acceleration highly depends on the source region where the particles come from. If new-born particles are inside the MPB, where the convection electric field is extremely weak, particles gain no significant acceleration and their paths are controled by the magnetic field therein. For the particles generated in the magnetosheath region, the strong convection electric field quickly accelerates them. After penetrating the MPB boundary, their motion is basically deflected by the magnetic field. The complicated **B** and **E** field configurations account for the complexity of the pickup ion distribution. Given the fact that the particle transport is strongly affected by the electromagnetic environment, the velocity space distribution can thus be used as a unique tool to probe Mars-solar wind interaction processes. In general, the kinetic effects due to the large gyroradius of high-energy ions around the unmagnetized planet are important and deserve a particular attention for the Mars pickup ion dynamics.

[50] **Acknowledgments.** This work was supported by NASA grants NNX07AF37G, NASW-00003, and NNG04G055G.

[51] Wolfgang Baumjohann thanks Janet Luhmann and Thomas Cravens for their asssistance in evaluating this paper.

References

Acuña, M. H., et al. (1998), Magnetic field and plasma observations at Mars: Initial results of the Mars Global Surveyor mission, *Science*, *279*, 1676.

Arkani-Hamed, J. (2001), A 50-degree spherical harmonic model of the magnetic field of Mars, *J. Geophys. Res.*, *106*, 23,197.
Barabash, S., et al. (2007), Martian atmospheric erosion rates, *Science*, *315*, 501.
Birdsall, C. K., and A. B. Langdon (1985), *Plasma Physics Via Computer Simulation*, McGraw-Hill, New York.
Brecht, S. H. (1997), Hybrid simulations of the magnetic topology of Mars, *J. Geophys. Res.*, *102*, 4743.
Brecht, S. H., J. R. Ferrante, and J. G. Luhmann (1993), Three-dimensional simulations of the solar wind interaction with Mars, *J. Geophys. Res.*, *98*, 1345.
Cravens, T. E., et al. (1987), Electron impact ionization in the vicinity of comets, *J. Geophys. Res.*, *92*, 7341.
Cravens, T. E., A. Hoppe, S. A. Ledvina, and S. McKenna-Lawlor (2002), Pickup ions near Mars associated with escaping oxygen atoms, *J. Geophys. Res.*, *107*(A8), 1170, doi:10.1029/2001JA000125.
Harnett, E. M., and R. M. Winglee (2006), Three-dimensional multifluid simulations of ionospheric loss at Mars from nominal solar wind conditions to magnetic cloud events, *J. Geophys. Res.*, *111*, A09213, doi:10.1029/2006JA011724.
Kallio, E., and P. Janhunen (2002), Ion escape from Mars in a quasi-neutral hybrid model, *J. Geophys. Res.*, *107*(A3), 1035, doi:10.1029/2001JA000090.
Kallio, E., and H. Koskinen (1999), A test particle simulation of the motion of oxygen ions and solar wind protons near Mars, *J. Geophys. Res.*, *104*, 557.
Kallio, E., H. Koskinen, S. Barabash, C. M. C. Nairn, and K. Schwingenschuh (1995), Oxygen outflow in the Martian magnetotail, *J. Geophys. Res.*, *22*, 2449.
Lichtenegger, H., and E. Dubinin (1998), Model calculations of the planetary ion distribution in the Martian tail, *Earth Planets Space*, *50*, 445.
Lichtenegger, H., K. Schwingenschuh, E. Dubinin, and R. Lundin (1995), Particle simulation in the Martian magnetotail, *J. Geophys. Res.*, *100*, 21,659.
Liu, Y., A. F. Nagy, T. I. Gombosi, D. L. De Zeeuw, and K. G. Powell (1999), 3D multi-fluid MHD studies of the solar wind interaction with Mars, *Geophys. Res. Lett.*, *26*, 2689.
Luhmann, J. G. (1990), A model of the ion wake of Mars, *Geophys. Res. Lett.*, *17*, 869.
Luhmann, J. G. (1997), Correction to "The ancient oxygen exosphere of Mars: Implications for atmospheric evolution", *J. Geophys. Res.*, *102*, 1637.
Luhmann, J. G., and J. U. Kozyra (1991), Dayside pickup oxygen ion precipitation at Venus and Mars: Spatial distributions, energy deposition and consequences, *J. Geophys. Res.*, *96*, 5457.
Luhmann, J. G., and K. Schwingenschuh (1990), A model of the energetic ion environment of Mars, *J. Geophys. Res.*, *95*, 939.
Lundin, R., and S. Barabash (2004), Evolution of the Martian atmosphere and hydrosphere: Solar wind erosion studied by ASPERA-3 on Mars Express, *Planet. Space Sci.*, *52*, 1059.
Lundin, R., et al. (1990), ASPERA/Phobos-2 measurements of the ion outflow from the Martian ionosphere, *Geophys. Res. Lett.*, *17*, 873.
Ma, Y., and A. F. Nagy (2007), Ion escape fluxes from Mars, *Geophys. Res. Lett.*, *34*, L08201, doi:10.1029/2006GL029208.
Ma, Y., A. F. Nagy, K. C. Hansen, D. L. De Zeeuw, and T. I. Gombosi (2002), Three-dimensional multispecies MHD studies of the solar wind interaction with Mars in the presence of crustal fields, *J. Geophys. Res.*, *107*(A10), 1282, doi:10.1029/2002JA009293.
Ma, Y., A. F. Nagy, I. V. Sokolov, and K. C. Hansen (2004), Three-dimensional, multispecies, high spatial resolution MHD studies of the solar wind interaction with Mars, *J. Geophys. Res.*, *109*, A07211, doi:10.1029/2003JA010367.
Modolo, R., G. M. Chanteur, E. Dubinin, and A. P. Matthews (2005), Influence of the solar EUV flux on the Martian plasma environment, *Ann. Geophys.*, *23*, 433.
Nagy, A. F., M. W. Liemohn, J. L. Fox, and J. Kim (2001), Hot carbon densities in the exosphere of Mars, *J. Geophys. Res.*, *106*, 21,565.
Nagy, A. F., et al. (2004), The plasma environment of Mars, *Space Sci. Rev.*, *111*, 33.
Sauer, K., and E. Dubinin (2000), The nature of the Martian obstacle boundary, *Adv. Space Res.*, *26*(10), 1633.
Sauer, K., K. Baumgärtel, I. Axnäs, and N. Brenning (1990), A fluid simulation of the AMPTE solar wind lithium release, *Adv. Space Res.*, *10*(7), 95.
Verigin, M. I., et al. (1991), Ions of planetary origin in the Martian magnetosphere (Phobos-2/Taus experiment), *Planet. Space Sci.*, *39*, 131.
Zhang, M. H. G., J. G. Luhmann, S. W. Bougher, and A. F. Nagy (1993), The ancient oxygen exosphere of Mars: Implications for atmospheric evolution, *J. Geophys. Res.*, *98*, 10,915.

D. L. De Zeeuw, X. Fang, J. U. Kozyra, M. W. Liemohn, A. F. Nagy, and T. H. Zurbuchen, Space Physics Research Laboratory, University of Michigan, 2455 Hayward Street, Ann Arbor, MI 48109-2143, USA. (darrens@umich.edu; xhfang@umich.edu; jukozyra@umich.edu; liemohn@umich.edu; anagy@umich.edu; thomasz@umich.edu)

Y. Ma, Institute of Geophysics and Planetary Physics, University of California, Los Angeles, CA 90095, USA. (yingjuan@igpp.ucla.edu)